Inorganic Chemistry

Article

pubs.acs.org/IC

Unichromophoric Platinum-Acetylides That Contain Pentiptycene Scaffolds: Torsion-Induced Dual Emission and Steric Shielding of Dynamic Quenching

Che-Jen Lin, Chih-Yuan Chen, Sandip Kumar Kundu, and Jye-Shane Yang*

Department of Chemistry, National Taiwan University, No 1, Sec 4, Roosevelt Rd, Taipei 10617, Taiwan

Supporting Information

ABSTRACT: The effect of the rigid bulky pentiptycene scaffolds on the photoluminescence, redox properties, and oxygen sensing behavior of unichromophoric Pt-acetylides is reported. When the pentiptycene groups are near the $Pt(PBu_3)_2$ center, the Pt-acetylides display both blue fluorescence and green phosphorescence with long phosphorescence lifetimes (90−202 μs) in THF. Their phosphorescence intensity is highly sensitive to molecular oxygen, and the emission color depends on the concentration of not only oxygen but also the complexes, which allows a feasible determination of oxygen in the range of 1−5% air volume. The dynamic quenching rate constants decrease linearly with increasing the number of pentiptycene groups, revealing the steric shielding effect of the peripheral rings of pentiptycene. A dependence of oxidation potential on the number of pentiptycene groups also revealed the steric shielding effect on the electron transfer between the complexes and the electrode. In a PMMA matrix, the dual emissive properties are diminished due to increased phosphorescence and decreased fluorescence intensity, and the phosphorescence lifetimes are significantly increased (up to ∼700 μs), leading to an "on−off" optical response to oxygen concentration. Both the dual emissive properties and long-lived triplet excitons are attributed to diminished spin−orbit couplings caused by twisting and steric shielding of the π-conjugated backbone around the Pt center.

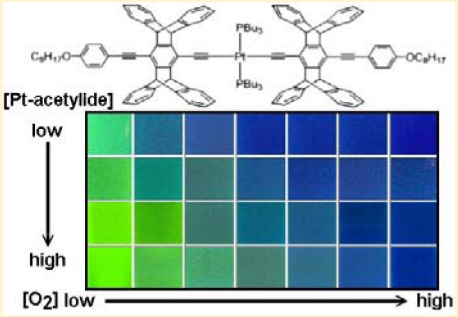

INTRODUCTION

Chromophores that display fluorescence−phosphorescence dual emissions at ambient temperature are attractive in both fundamental and technological points of view.[1−6] The dual emissive behavior requires a subtle balance of reaction rates between fluorescence and intersystem crossing (ISC) in the lowest singlet excited state (S_1) and between phosphorescence and nonradiative decays in the lowest triplet excited state (T_1). Because of a much longer lifetime for T_1 versus S_1, the intensity of phosphorescence is much more sensitive than that of fluorescence to molecular oxygen. Therefore, these dual emissive chromophores are potential ratiometric luminescent probes for the detection of oxygen in biological and environmental systems.[2,4−7] Ratiometric luminescence detection is a self-referencing method and superior to the luminescence quenching or amplification approach. Many ratiometric oxygen sensors have been designed by integrating fluorescent and phosphorescent chromophores.[2,8−10] One potential problem of these bi- or multichromophoric systems is the chromophore-dependent photobleaching activity, which challenges the self-referencing reliability. While dual emissive unichromophores can circumvent this problem, examples of unichromophore-based ratiometric oxygen probes are rather limited.[2,4−7,11]

Photoluminescent transition metal complexes are an important class of phosphorescent materials,[12−15] which have been extensively studied as oxygen probes.[16−24] In principle, an appropriate attenuation of the ISC efficiency of a known phosphorescent transition metal complex could lead to dual emissive systems. Of the various photoluminescent transition metal complexes, the square-planar d^8 Pt(II) complexes are ideal candidates because of the relatively weaker spin−orbit coupling exerted by the Pt atom.[2,3] A known strategy to attenuate the ISC efficiency for Pt complexes is to extend the π-conjugation length of the ligand.[3,4,25,26] For example, the Pt-acetylides $[trans\text{-}Pt(PBu_3)_2((—C{\equiv}C—C_6H_4)_n—H)_2]$ display a decreased triplet quantum yield through the series (n = 1 → 3). While the quantum yield of fluorescence (Φ_f) is as low as 0.001 at n = 2, it is comparable to that of phosphorescence (Φ_p) at n = 3, where $\Phi_p \sim \Phi_f \sim 0.016$.[25] Despite the potential dual emissive properties, Pt-acetylides have not been investigated as ratiometric oxygen probes.

Pentiptycene is an H-shaped member of the iptycene family.[27] Because of the rigid and nonplanar scaffold, pentiptycene has been incorporated into π-conjugation oligomers[28] and polymers[29,30] to diminish interchain π-stacking and thus the fluorescence quenching in thin solid films. The same concept has also been applied to Pt-acetylide polymers to explore the intra- versus interchain effects in the triplet excited states.[31] Although the torsional constraint between the bulky pentiptycene groups and the neighboring $Pt(PBu_3)_2$ units in

Received: July 1, 2013
Published: January 3, 2014

   dx.doi.org/10.1021/ic4025052 | Inorg. Chem. 2014, 53, 737−745

Chart 1

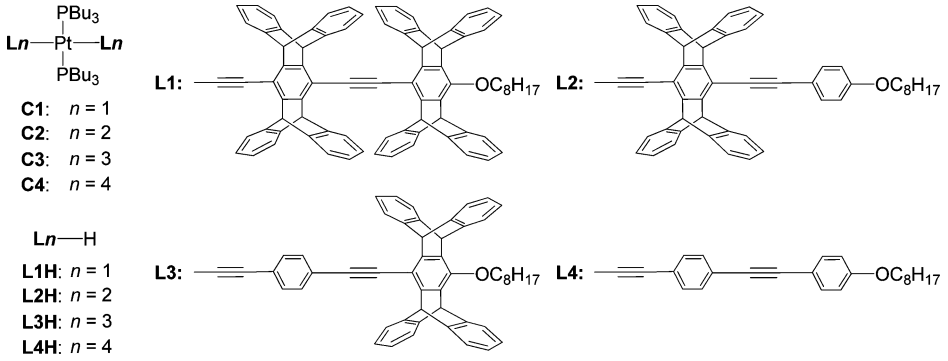

Scheme 1

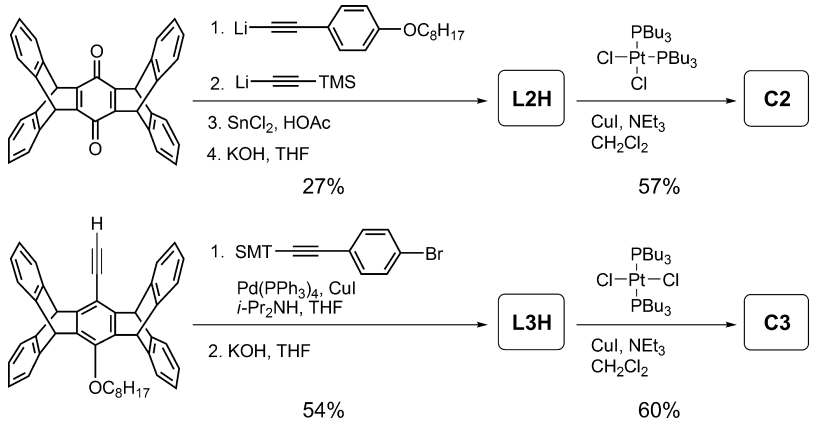

the pentiptycene-derived Pt-acetylide polymer was noticed, such a conformational effect on the photophysical properties has not been fully addressed.

We report herein the effect of pentiptycene scaffolds on the photophysical properties of Pt-acetylides (Chart 1). We observed that decreasing the torsional flexibility of the arene near the Pt center of Pt-acetylides could attenuate the ISC efficiency and thus create dual emission. This is manifested by the Pt-acetylides **C1**–**C4**, in which **C1** and **C2** are dual emissive but **C3** and **C4** display essentially only phosphorescence. The key structural feature in the former two species is the bulky pentiptycene groups in neighbor of the PtP_2C_2 unit. As a result of the long phosphorescence lifetimes (90–202 μs), **C1** and **C2** in dilute THF solutions display nearly complete phosphorescence quenching at low oxygen conditions, resulting in luminescence color change from green to blue. The oxygen quenching dynamics of **C1**–**C4** also reveals an intriguing steric shielding effect exerted by the pentiptycene scaffolds. The solid-state photophysical properties and oxygen sensing behavior of **C1**–**C4** in a PMMA matrix were also investigated for comparison.

RESULTS AND DISCUSSION

Synthesis. The synthesis of **C1**–**C4** adopted Hagihara's method[32] using the corresponding ligands **L1H**–**L4H** and the Pt substrates [*cis*-$PtCl_2(PBu_3)_2$] (for **C1** and **C2**) and [*trans*-$PtCl_2(PBu_3)_2$] (for **C3** and **C4**). The two synthetic protocols were illustrated in Scheme 1, as represented by the cases of **C2** and **C3**, respectively. The ligand **L1H** was previously reported,[33] and **L2H** was synthesized through the same protocol: sequential nucleophilic addition of arylacetylide and trimethylsilylacetylide to pentiptycene quinone followed by aromatization with $SnCl_2$ and then by removal of the trimethylsilyl (TMS) group under basic condition. Ligands **L3H** and **L4H** were synthesized through the Sonogashira reactions with octylarylacetylene and trimethylsilyl bromoaryl acetylene followed by removal of the TMS group (Supporting Information Scheme S1). Whereas **L3H** and **L4H** react readily with [*trans*-$PtCl_2(PBu_3)_2$] to form **C3** and **C4**, respectively, the corresponding reactions with **L1H** and **L2H** only led to monosubstituted intermediates [*trans*-$PtCl(Ln)(PBu_3)_2$] (n = 1 and 2). The poor reactivity of the intermediates with **L1H** and **L2H** reveals the pentiptycene effect on this metalation reaction. Instead, **C1** and **C2** were prepared with the more reactive [*cis*-$PtCl_2(PBu_3)_2$] substrate followed by *cis*-to-*trans* isomerization. The isomerization occurred efficiently even at room temperature, indicating a low energy barrier. The ^{1}H, ^{13}C, and ^{31}P NMR spectra of **C1**–**C4** are provided as Supporting Information (Figures S1–S12). The *trans*-configuration of **C1**–**C4** is confirmed by ^{31}P NMR spectroscopy; the chemical shifts of the PBu_3 groups, which are in the range 3.33–4.29 ppm, and the coupling constants for Pt–P, which are in the range 2342–2350 Hz, are similar to those observed for [*trans*-$Pt(PBu_3)_2(—C{\equiv}C—C_6H_5)_2$].[26] On the basis of the order of chemical shifts **C1** (4.29 ppm) > **C2** (4.19 ppm) > **C3** (3.53 ppm) > **C4** (3.33 ppm), a magnetic deshielding of the PBu_3 groups by the neighboring pentiptycene groups is evidenced.

Photophysical Properties. The absorption spectra of **C1**–**C4** in THF are shown in Figure 1a. The absorption maxima are in the small range 352–357 nm for all four complexes (Table 1). However, they can be divided into two groups in terms of the spectral features. The group consisting of **C1** and **C2**

dx.doi.org/10.1021/ic4025052 | Inorg. Chem. 2014, 53, 737–745

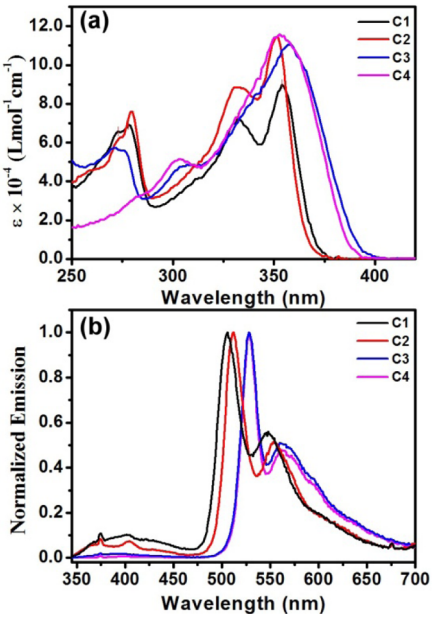

Figure 1. (a) Absorption and (b) normalized emission spectra of **C1**–**C4** in THF.

(group I) displays a narrower, more structured, and less tailing long-wavelength absorption band than the other group containing **C3** and **C4** (group II). The spectral differences between the two groups could be attributed to the difference in steric interactions between the PtP_2C_2 unit and the neighboring arenes, in which an increased conformational constraint toward "twisted" geometries is expected for group I relative to group II (Figure 2). The narrower and blue-shifted absorption onset for group I versus II could then be attributed to a diminishment of rotational heterogeneity along the **L*n***–Pt–**L*n*** backbone by reducing the population of the coplanar rotamers. It is well-documented that the more planar the rotamer of phenyleneethynylene oligomers is, the lower energy it absorbs.[33,34] A similar argument has been proposed by Schanze and coworkers for a pentiptycene-derived Pt-acetylide polymer.[31] It is also possible that the Pt-pentiptycene twisting might weaken the contribution of metal-to-ligand charge transfer (MLCT) to the S_1 state. A MLCT absorption band is generally broader and less structured than an LC band. However, according to the structured phosphorescence spectra (see below), the MLCT character for the T_1 state should be minor for both groups. For the short-wavelength absorption bands in 250–280 nm, they can be attributed to the $\pi \rightarrow \pi^*$ transition of the peripheral nonconjugated phenylene rings of pentiptycene, as the intensity is proportional to the number of pentiptycene moieties in the complexes.

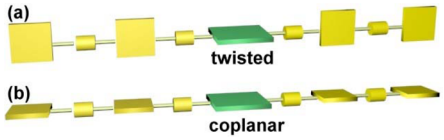

Figure 2. Schematic drawings of the **L*n***–Pt–**L*n*** backbone conformation for (a) twisted and (b) coplanar geometry between the PtP_2C_2 plane (green) and the arene of ligands (yellow).

The emission properties of **C1**–**C4** were investigated in dilute THF solutions at room temperature. The two groups defined above for absorption also differ from one another in the emission properties. For **C1** and **C2** (group I), the emission spectra have dual bands with maxima at ~400 and ~510 nm, and the latter band is more intense and structured (Figure 1b). The two emission bands have distinct decay times, which is <4.0 ns for the 400-nm band and ≥90 μs for the 510-nm band in degassed solutions, assignable to fluorescence and phosphorescence, respectively. The total luminescence quantum yield is near 0.07 with the Φ_p/Φ_f ratio near 5 (Table 1). In contrast, complexes **C3** and **C4** (group II) display only a single phosphorescence band with negligible fluorescence (Φ_f < 0.001). The phosphorescence properties are nearly the same for both complexes (Table 1), which indicates that the terminal arenes being either phenylene or pentiptycene is unimportant. Compared to group I, group II displays larger phosphorescence quantum yields (Φ_p ~ 0.20) at longer wavelength (λ_p = 528 nm). The phosphorescence lifetime (τ_p ~160 μs) is longer than that of **C1** (90 μs) but shorter than that of **C2** (202 μs). It is also noted that the τ_p is much larger for **C4** than the parent Pt-acetylide [*trans*-$Pt(PBu_3)_2$(—C≡C—C_6H_4—C≡C—$C_6H_5)_2$] (~42 μs in benzene).[25] If the prolonged lifetime observed for **C4** versus the parent system is not caused by different degassing or solvent conditions, it shows a significant alkoxy substituent effect. Long-lived triplet states of analogous Pt-acetylides containing alkyl or alkoxy substituents on the phenylene rings have been reported.[35]

The influence of pentiptycene groups on the phosphorescence quantum yield and lifetime of Pt-acetylides **C1**–**C4** deserves further analysis. The magnitude of spin–orbit coupling and that of S_1–T_1 energy gap (ΔE_{ST}) and the electronic nature of T_1 are three important parameters for consideration.[36,37] Large spin–orbit couplings would enhance the triplet yield and thus decrease the Φ_f. A small ΔE_{ST} facilitates not only the formation of T_1 but also the increase of Φ_p due to enhanced phosphorescence rate (i.e., shorter τ_p). For the electronic character of T_1, the τ_p is increased with increasing the LC character. It has been shown that the T_1 state of Pt-acetylides is less delocalized than the S_1 state and is confined in the Pt–**L*n*** segment.[38,39] As the structural difference

Table 1. Photophysical[a] Data for C1–C4 in THF

compd	λ_{abs} (nm)	ε (L mol^{-1} cm^{-1})	λ_f (nm)	Φ_f	τ_f[b] (ns)	λ_p[c] (nm)	Φ_p	τ_p (μs)	K_{SV} (bar^{-1})	k_q (μs^{-1} bar^{-1})
C1	354	90 000	402	0.012	0.39 (97%) 3.61 (3%)	506 (548)	0.047	90	430 ± 60	5
C2	352	115 000	402	0.011	1.07 (92%) 2.74 (8%)	512 (553)	0.064	202	2600 ± 180	13
C3	357	111 000	398	<10^{-3}	<0.2	528 (560)	0.20	159	2300 ± 200	15
C4	353	116 000	398	<10^{-3}	<0.2	528 (560)	0.20	160	3600 ± 90	23

[a]Wavelength of maximum for absorption (λ_{abs}), fluorescence (λ_f), and phosphorescence (λ_p), extinction coefficients (ε) at λ_{abs}, quantum yields of fluorescence (Φ_f) and phosphorescene (Φ_p), lifetimes of fluorescence (τ_f) and phosphorescence (τ_p), and Stern–Volmer constants (K_{SV}) and rate constants (k_q) for the phosphorescence quenching by O_2. [b]The percentage of each component is shown in parentheses. [c]The second vibronic bands are given in parentheses.

dx.doi.org/10.1021/ic4025052 | *Inorg. Chem.* 2014, 53, 737–745

among **C1**−**C4** is the location and number of pentiptycene groups, the major pentiptycene effect is believed to constrain the planarization relaxation of the conjugated backbone in the excited states. Regarding the fact that the degree of steric congestion is **C1** > **C2** > **C3** ∼ **C4** and the relative λ_p is in the opposite order **C1** (506 nm) < **C2** (512 nm) < **C3** = **C4** (528 nm), the observed λ_p might simply reflect the relative backbone planarity in T_1. Accordingly, the smaller Φ_p and larger Φ_f observed for group I versus II indicate that twisting the Pt-acetylides π-backbone could attenuate the spin−orbit couplings and/or increase the ΔE_{ST}. While a larger τ_p for **C2** relative to group II conforms to the scenario of a larger ΔE_{ST}, the smaller τ_p for **C1** might indicate an increased rate for nonradiative decays. These results appear to suggest that twisting of the Pt center from the **L*n*** planes slows down the $S_1 \rightarrow T_1$ ISC and that twisting within the **L*n*** moiety increases the rate of nonradiative decay for T_1. Further studies are required to confirm this hypothesis.

DFT Calculation. To strengthen the argument of the pentiptycene steric effect, DFT calculations (B3LYP[40−42] functional with 6-31G (d) for C, H, O, and P and SDD[43] basis set for Pt) were performed on **C2** and **C4**, in which the terminal $-OC_8H_{17}$ groups were replaced with the $-OCH_3$ to reduce the cost of calculation. The DFT-optimized structures show a coplanar π-conjugated backbone in the **L2** and **L4** moieties, and the internal phenylene rings are nearly perpendicular (90 ± 3°) to the central PtP_2C_2 plane in both **C2** and **C4**. According to the well-documented torsional studies on phenylene-ethynylene oligomers,[44] torsions about the $C_{sp2}-C_{sp}$ single bonds in **L*n*** should encounter a negligible barrier (<1.0 kcal mol^{-1}). Whereas constraining one of the **L*n*** planes coplanar to the central PtP_2C_2 plane raises the energy by only 0.71 kcal mol^{-1} for **C4**, it costs as much as 10.6 kcal mol^{-1} in the case of **C2**. The presence of strong Pt-pentiptycene steric interactions in the planarized form of **C2** is also evidenced by the distorted and bended geometry around Pt (Supporting Information Figure S13 and Table S1). The larger torsional freedom for **C4** versus **C2** is consistent with the broader and red-shifted absorption band.

The DFT-derived frontier molecular orbitals HOMO and LUMO of **C2** and **C4** are shown in Figure 3. Whereas the

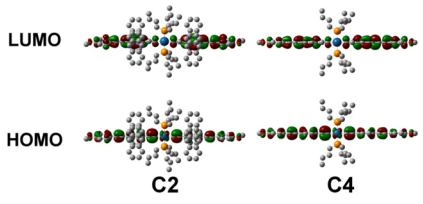

Figure 3. Frontier molecular orbitals of **C2** and **C4**.

HOMO is located at the **L*n***−Pt−**L*n*** backbone with the contribution of the Pt atom, the LUMO is mainly on the ligands. The HOMO → LUMO transition is expected to be mainly ligand-centered in nature with a minor MLCT character. The delocalized HOMO and LUMO also conform to a unichromophoric character of **C1**−**C4** (Supporting Information Figure S14).

Electrochemical Properties. To investigate the effect of Pt-pentiptycene steric interactions on the ground-state electronic properties of **C1**−**C4**, the redox potentials of **C1**−**C4** and **L1H**−**L4H** were determined with cyclic voltammetry (CV) and differential pulse voltammetry (DPV) in CH_2Cl_2 solution. Figure 4 shows the CV and DPV profiles of **C1**−**C4**

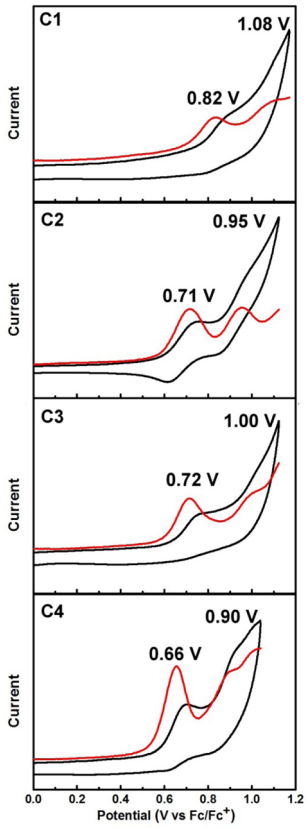

Figure 4. Cyclic (black) and differential pulse (red) voltammograms of **C1**−**C4** in CH_2Cl_2 with supporting electrolyte 0.01 M Bu_4NPF_6 at a scan rate of 50 mV s^{-1}.

with the redox potential relative to that of the ferrocene/ferrocenium (Fc/Fc^+) couple. For all four cases, two anodic waves are present, and no cathodic processes occur within the solvent window (±1.2 V). The first oxidation potential (E_{ox1}) is in the order **C1** (0.82 V) > **C3** (0.72 V) ∼ **C2** (0.71 V) > **C4** (0.66 V). That the E_{ox1} of **C2** is similar to that of **C3** rather than **C1** clearly indicates that the Pt-pentiptycene torsional constraint in **C1** and **C2** but not in **C3** and **C4** plays a minor role in determining the value of E_{ox1}. It appears that the number of pentiptycene groups, which is 4−2−2−0 through the compound series **C1** → **C4**, is more important, as **C2** and **C3** have the same number of pentiptycene groups and meanwhile similar value of E_{ox1}. This might suggest that the heterogeneous electron transfer (HET) between electrode and the substrates is significantly affected by the bulkiness of substrates due to the pentiptycene groups. The phenomenon of HET retarding by bulky substituents has been reported for the reduction of nitroalkane and diketone.[45,46] The relationship between E_{ox1} and number of pentiptycene groups also indicates a delocalized nature of the redox state, which is consistent with the HOMO character (Figure 3) and the assignment for related Pt complexes.[47] For the second oxidation potential (E_{ox2}), it is larger than the E_{ox1} by 0.26 ± 0.02 V for all four cases (Figure 4). This again indicates that the Pt-pentiptycene torsional constraint has little effect on the electronic communication along the **L*n***−Pt−**L*n*** backbone in the first oxidation state. In contrast, the oxidation potentials for the free ligands are in the

dx.doi.org/10.1021/ic4025052 | *Inorg. Chem.* 2014, 53, 737−745

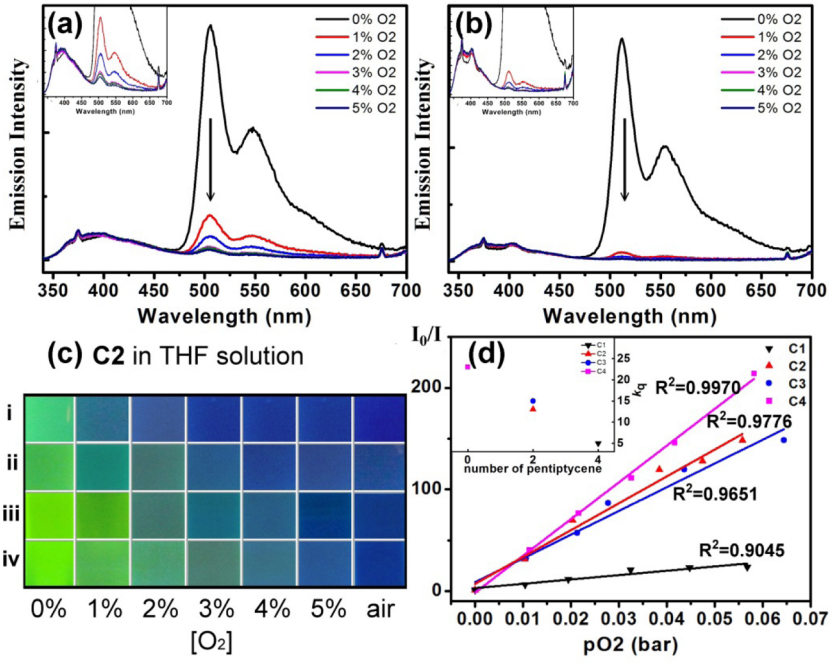

Figure 5. Dependence of emission spectra of (a) **C1** and (b) **C2** (3×10^{-6} M) in THF on the concentration of O_2 at 1−5%, (c) the color of emission of **C2** in the concentration of (i) 3×10^{-6} M, (ii) 9×10^{-5} M, (iii) 1.8×10^{-4} M, and (iv) 3.6×10^{-4} M at different volumetric ratio of molecular oxygen (O_2) in the mixture of O_2 and N_2, and (d) the Stern−Volmer plots of the phosphorescence intensity against the pressure of O_2 for **C1**−**C4** (3×10^{-6} M). The insets in parts a and b are the enlarged spectra, and in part d it is the correlation between number of pentiptycene and k_q.

order **L1H** (1.18 V) = **L3H** (1.18 V) > **L2H** (1.05 V) ~ **L4H** (1.02 V) (Supporting Information Figure S15). This might suggest that the octyloxy-substituted arene, which is the unsubstituted phenylene ring in **L2H** and **L4H** but the bulky pentiptycene group in **L1H** and **L3H**, plays a critical role in the redox process. In other words, the electron-donating octyloxy group directs the redox process for the free ligands so that the arene with the octyloxy substituent is important in determining the oxidation potential; however, in the Pt complexes **C1**−**C4**, both arenes of the ligands are important in determining the redox potential. The oxidation potential is raised whenever the directing arenes are pentiptycene relative to phenylene rings.

Oxygen Sensing. The features of dual emissions with relatively stronger phosphorescence intensity and long phosphorescence lifetimes render **C1** and **C2** ideal candidates as ratiometric oxygen probes. In this context, their ratiometric oxygen sensing behavior was investigated in THF solutions (3×10^{-6} M). As shown in Figure 5a,b, the phosphorescence but not the fluorescence intensity of **C1** and **C2** is highly sensitive to oxygen in the surroundings. The phosphorescence is essentially quenched at 1% of oxygen in the air volume. This is accompanied with a color change from green to blue in the luminescence (panel i in Figure 5c). Such a high sensitivity of the phosphorescence to oxygen prompted us to investigate the concentration effect of the complex **C2**. It is expected that increasing the concentration of **C2** would need a higher concentration of oxygen to reach a full phosphorescence quenching. Therefore, the detection range of **C2** as a ratiometric oxygen probe can be extended to an oxygen concentration larger than 1%. Indeed, as shown in panels ii−iv of Figure 5c, a semiquantitative visual detection of oxygen can be extended to 5% in the air volume. The Stern−Volmer plots in Figure 5d show a linear relation between oxygen pressure and intensity of phosphorescence, indicating a simple dynamic quenching mechanism.[18,48] The Stern−Volmer constants (K_{SV}), namely, the slopes of the plots, are significantly larger (430−2600 bar^{-1}) than previously reported systems.[2,4−6,11] As K_{SV} is a product of the phosphorescence lifetime (τ_p) and the bimolecular quenching constant (k_q), the high efficiency of phosphorescence quenching by oxygen is mainly due to the large τ_p values (90−202 μs).

For the purpose of mechanistic elucidation, the phosphorescence quenching of **C3** and **C4** was also investigated under the same conditions (Table 1 and Figure 5d). The K_{SV} values of **C3** and **C4** are comparable or even larger than that of **C2**, although their τ_p values are somewhat lower (~160 μs). Accordingly, the k_q values (in unit of $bar^{-1}\mu s^{-1}$) are in the order **C1** (5) < **C2** (13) < **C3** (15) < **C4** (23). The k_q values are inversely proportional to the number of pentiptycene groups in complexes, which is 4−2−2−0 through the compound series **C1** → **C4**. Regarding the high probability of quenching at any collision between oxygen and the exciton,[49] the **L*n***-dependent k_q values indicate that the lateral nonconjugated phenylene groups of pentiptycene shield the triplet exciton from interacting with oxygen. This is reminiscent of the application of iptycenes as steric protecting group for stabilizing a reactive center such as carbenes.[50]

Solid-State Behavior. To compare the photoluminescence behavior of **C1**−**C4** in the solid state versus in solution phase, the photophysical properties of **C1**−**C4** in a poly(methylmethacrylate) (PMMA) matrix under pure nitrogen atmosphere have been determined (Figure 6), and pertinent data are summarized in Table 2. Both the absorption and phosphorescence maxima undergo small shifts ($\Delta\lambda$ = 0−3 nm) on going from THF solutions to the thin solid films, which indicates the absence of significant intermolecular interactions in the PMMA films. The shoulder in the region above 400 nm of absorption spectra could be attributed to light scattering due to nonhomogeneity of the films, although the contribution of changes in molecular conformations toward more planar

dx.doi.org/10.1021/ic4025052 | Inorg. Chem. 2014, 53, 737−745

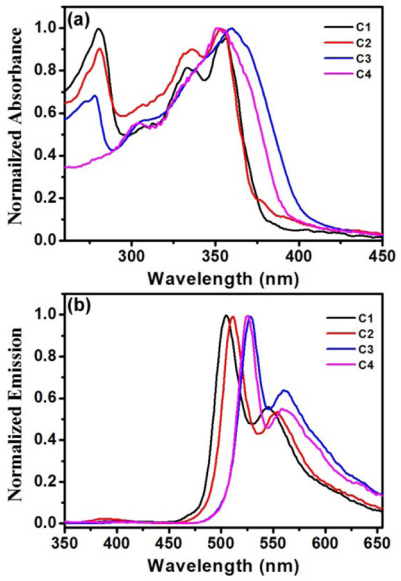

Figure 6. Normalized (a) absorption and (b) emission spectra of **C1**–**C4** in a PMMA matrix at room temperature under nitrogen atmosphere.

geometry cannot be completely excluded. The phenomenon of dual emission for **C1** and **C2** observed in THF solutions is significantly diminished in the PMMA films, because the fluorescence is decreased and the phosphorescence is enhanced, indicating an increased spin–orbit coupling in the latter. Under the oxygen-free condition, the Φ_p/Φ_f ratio is as high as 55–100 in the thin films, which makes the ratiometric optical detection less practical (vide infra). By following the concept of torsion-induced attenuation of spin–orbit coupling discussed above, a reduced Pt-pentiptycene torsion angles and/or torsional flexibility might be responsible for the changes in dual emissive properties for the complexes in the PMMA matrix. In contrast to the increase of Φ_p by ~50% for **C1** and **C2** on going from THF solutions to thin solid films, the Φ_p is decreased by 50% in the cases of **C3** and **C4**. Evidently, the Pt-pentiptycene steric effect on phosphorescence is more pronounced in the thin films. The τ_p is also largely affected by the medium, and it is generally increased in the thin films versus the THF solutions, although a minor shorter-lived component is present for **C1**–**C3** in the former condition. The phenomenon of an increased τ_p in a thin film versus dilute solution is intriguing in view of the fact that the inevitable impurities and/or energy traps in a thin film generally reduce the lifetime of the doped excitons.[29] Provided that the different degassing condition is not responsible for the difference in τ_p, the larger τ_p values in PMMA could be attributed to more effective shielding of the triplet exciton to quenchers. The current results show that the photophysical properties of **C1**–**C4** are highly sensitive to the environments.

Figure 7 shows the solid-state emission spectra and images of **C2** in a PMMA thin film under atmosphere of varied oxygen/

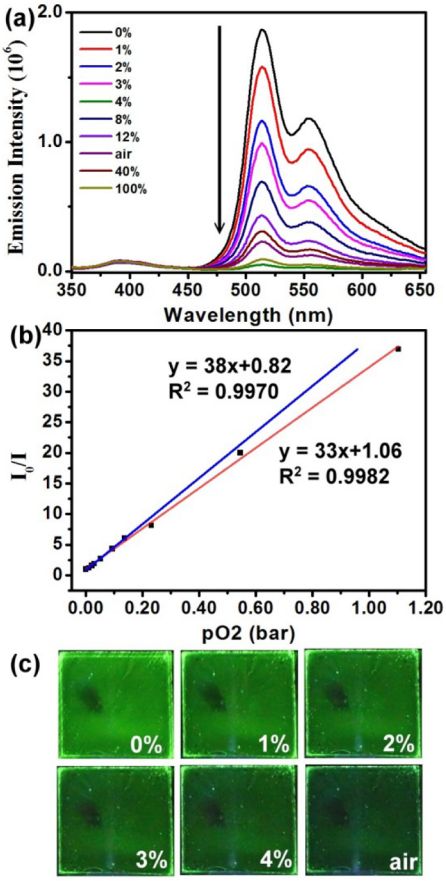

Figure 7. (a) Emission spectra, (b) the Stern–Volmer plot, and (c) emission images for **C2** in a PMMA matrix at varied O_2 concentration in O_2/N_2 (v/v) mixed gas. The small dark region on the left-hand side of the images corresponds to an intentionally prepared nonemissive region with a triplet quencher (a drop of 10% benzophenone in dichloromethane) as an internal reference.

nitrogen concentration. Like the case in THF solutions, the phosphorescence but not the fluorescence intensity is sensitive to the oxygen concentration. However, compared to the case in THF solutions, the sensitivity of phosphorescence in response to oxygen is much lower so that phosphorescence remains to dominate the emission even under the open air; a full quenching of the phosphorescence requires the condition of 100% oxygen atmosphere. The Stern–Volmer constant (K_{SV} = 33 ± 0.5 bar^{-1}) is ~80-fold lower than that in THF solutions (Figure 7b). By using the pre-exponential weighted mean lifetime (~630 μs),[18] the quenching rate constant k_q is 0.05 μs^{-1} bar^{-1}, which is 260-fold lower than that in THF (Table 1). This could be attributed to limited oxygen permeability of the

Table 2. Photophysical Properties[a] of C1–C4 in a PMMA Matrix

compd	λ_{abs} (nm)	λ_f (nm)	λ_p (nm)	Φ_f	Φ_p (air)	Φ_p (N_2)	τ_p (air) (μs)	τ_p (N_2) (μs)
C1	356	395	505 (545)	0.001	0.01	0.10	37	123 (26%) 596 (74%)
C2	354	391	511 (553)	0.002	0.01	0.11	8 (12%) 40 (88%)	46 (10%) 699 (90%)
C3	360	na[b]	528 (561)	$<10^{-3}$	0.02	0.10	9 (15%) 48 (85%)	63 (36%) 245 (64%)
C4	353	na[b]	526 (560)	$<10^{-3}$	0.02	0.09	50	215

[a]Notations are the same as in Table 1. [b]Not available because of extremely weak intensity.

dx.doi.org/10.1021/ic4025052 | Inorg. Chem. 2014, 53, 737–745

PMMA films.[51−53] Nevertheless, the Stern−Volmer plot of the whole data is linear with a better fit than the plot with data of low oxygen concentrations (pO_2 < 0.2 bar), indicating that the dynamic quenching is in operation and the films have good homogeneity. Because of the weak fluorescence, the response of photoluminescence of the films is more like an "on−off" type (Figure 7c) rather than the ratiometric color change as seen in the THF solutions (Figure 5c). A solution of this limitation might rely on further engineering of thin solid films in different matrix or solid support and on a more sophisticated setup and readout system such as fiberoptic sensory devices.[54]

The relative Φ_p and τ_p for **C1**−**C4** under the pure nitrogen and air conditions (Table 2) also deserve a comment. For **C1** and **C2**, the Φ_p is lowered by 10 times on going from pure nitrogen to air, but it is lowered by only 5 times for **C3** and **C4**. Such a relationship is roughly proportional to the corresponding changes in τ_p. Thus, the data again show that the magnitude of phosphorescence lifetime plays a key role in the sensitivity of oxygen sensing.

CONCLUSION

This work uncovers the iptycene substituent effect on the electronic properties of Pt-acetylides [*trans*-Pt(PBu_3)$_2$(—C≡C—Ar—C≡C—Ar′—OC_8H_{17})$_2$] (Ar and Ar′ = phenylene or pentiptycene) and on the electronic interactions between the Pt complexes and the environments (oxygen and electrode). The results show that the **L*n***−Pt−**L*n*** backbone conformation plays an important role in determining the excited-state decay behavior of Pt-acetylides. Steric torsion and shielding of the backbone result in dual emission of fluorescence and phosphorescence and long phosphorescence lifetime. This in turn leads to a highly sensitive phosphorescence response to oxygen. In addition, the pentiptycene scaffolds impose a steric shielding not only to the diffusion of oxygen to the triplet exciton but also to the electron transfer to the electrode. The structure−property relationship revealed herein might prove values for developing new Pt-acetylides as long-lived triplet sensitizers and ratiometric probes.

EXPERIMENTAL SECTION

General Methods. Electronic spectra were recorded at room temperature (23 ± 1 °C). UV−vis spectra were recorded using a Cary300 double beam spectrophotometer. Emission spectra were recorded using an Edinburgh FLS920 spectrometer at ambient temperature, and corrected for the response of the detector. A N_2-outgassed (5 min) solution of anthracene (λ_{ex} = 338 nm, Φ_f = 0.27 in hexane)[55] was used as standard for emission quantum yields determination, corrected with solvent refractive index, of compounds in a solution under three freeze−pump−thaw cycles. The optical density of all solutions was about 0.1 at the wavelength of excitation, and an error of 10% is estimated for emission quantum yields. Phosphorescence decays were measured by means of the Edinburgh FLS920 spectrometer apparatus with a μF900, a pulsed Xenon flashlamp, with a R928 detector, and range of measured decay is from 1.5 μs to 10 s. The goodness of nonlinear least-squares fit for phosphorescence was judged by the reduced χ^2 value (<1.2 in all cases), the randomness of the residuals, and the autocorrelation function. The solid-state electronic spectra and lifetime measurements were conducted with drop-cast films formed inside a quartz cuvette prepared with a $CHCl_3$ solution (0.5 mL) containing the complex (1.0 mg) and PMMA (10.0 mg). The absolute quantum yields for samples in air were determined using an integrating sphere (150 mm diameter, $BaSO_4$ coating) of Edinburgh Instruments by the Edinburgh FLS920 spectrometer. The quantum yields for samples in other oxygen concentrations were obtained from the corresponding emission spectra relative to the spectra in air.

The cyclic voltammetry (CV) and differential pulse voltammetry (DPV) were performed at a sweep rate of 50 mV s^{-1} on a CHI 612B electrochemical analyzer, and the electrochemical cells adopted a glassy carbon as the working electrode, a Pt wire as the counter electrode, an Ag wire as the reference electrode, and 0.01 M Bu_4NPF_6 as electrolyte. The substrates are ∼0.1 mM in CH_2Cl_2, and the solutions were outgassed by N_2 before measurement. All oxidation potentials were determined by DPV and calibrated with the ferrocene/ferrocenium (Fc/Fc^+) redox couple. The ^1H, ^{13}C, and ^{31}P NMR spectra were collected using Varian Mercury A-400 or Bruker DPX 400-MHz spectrometer. The ^{31}P NMR chemical shifts determined for the Pt complexes are referenced to 85% H_3PO_4(aq) in $CDCl_3$. IR spectra were recorded by Varian 640-IR. High-resolution mass spectra were collected by JEOL JMS-700 at National Central University. Elemental analysis was carried out on Heraeus VarioEL-III analyzer at National Taiwan University.

Calculations. Density functional theory (DFT) calculations were performed using Guassian 09 program[56] package at the B3LYP/6-31G(d,p) level[40−42] for the ligands. For the complexes, the Stuttgart−Dresden (SDD)[43] basis set was used with a relativistic effective core potential for Pt, and all ligand atoms (C, H, P, and O) were described by the B3LYP 6-31G(d) basis set. The optimized ground-state geometries were investigated by varying dihedral angle between every four atoms except for hydrogen atoms. The coplanar geometry was obtained by fixing the dihedral angle between the Pt−P bond and the neighboring arene C−C bond (i.e., $\psi_{C3-C4-Pt-P}$ in Supporting Information Table S1) to be 0° followed by the same protocol of ground-state geometry optimization.

Oxygen Sensing. Flow rate of N_2 and O_2 was controlled by single tube flowmeter (AALBORG), and the volumetric flow rate was monitored by bubble flowmeter. For the solution-phase sensing, the THF solutions were saturated with N_2 and O_2 at different air volume ratio by bubbling (flow rate = 30 mL min^{-1}; time = 15 min). For the solid-phase sensing, the same drop-cast film of **C2** used for the measurements of electronic spectra was used. The emission images were taken with spin-cast films on quartz plates prepared with the same $CHCl_3$ solution used for the drop-cast films.

Materials. Solvents for organic synthesis were reagent grade or HPLC grade, but for spectra and quantum yield measurement they were all HPLC grade. All new compounds were characterized with ^1H and ^{13}C NMR and IR spectroscopy, mass spectrometry, and/or element analysis. The synthetic procedure and characterization data for **C1**−**C4** are provided in the following, and those for the ligands **L*n*H** and the intermediates are provided as Supporting Information.

General Procedure for Synthesis of C1−C4. To a mixture of the ligand **L*n*H** (0.10 mmol), CuI (0.003 g, 0.02 mmol), and *cis*-$PtCl_2(PBu_3)_2$ (for **C1** and **C2**) or *trans*-$PtCl_2(PBu_3)_2$ (for **C3** and **C4**) (0.03 g, 0.05 mmol) in a 50-mL Schlenk flask was added triethylamine (5.0 mL) and CH_2Cl_2 (10.0 mL), and then the mixture was stirred under nitrogen at ambient temperature for 12 h. The solvent was removed under reduced pressure, and the residue was purified by column chromatography with CH_2Cl_2/hexane (1:3, v/v) as eluent afforded the desired compounds **C1**−**C4**.

Complex ***C1***. White solids: yield 45%; mp >300 °C (with decomposition). ^1H NMR (400 MHz, $CDCl_3$) δ: 0.97−1.05 (m, 24H), 1.42−1.64 (m, 28H), 1.72−1.73 (m, 4H), 1.96−2.10 (m, 16H), 2.47 (m, 12H), 4.06 (t, J = 6.8 Hz, 4H), 5.81 (s, 4H), 6.23 (s, 4H), 6.30 (s, 4H), 6.31 (s, 4H), 7.02−7.04 (m, 32H), 7.40−7.44 (m, 16H), 7.56−7.58 (m, 16H). ^{13}C NMR (100 MHz, $CDCl_3$) δ: 14.4, 22.9, 24.6, 26.6, 27.1, 29.6, 29.8, 30.8, 32.1, 35.0, 48.5, 52.5, 53.0, 69.7, 76.3, 85.1, 91.0, 91.3, 95.4, 101.3, 104.2, 111.7, 123.4, 123.6, 123.8, 125.2, 125.4, 131.4, 135.5, 142.5, 143.1, 145.0, 145.1, 145.6, 145.8. ^{31}P NMR (162 MHz, CDC_{l3}) δ: 4.29 ($^1J_{P-Pt}$ = 2348 Hz). IR (KBr): 2085 (C≡C) cm^{-1}. HRMS calcd for $C_{184}H_{168}O_2P_2Pt-H^+$: 2666.2219. Found: 2666.2229.

Complex ***C2***. White solids: yield 57%; mp >300 °C (with decomposition). ^1H NMR (400 MHz, $CDCl_3$) δ: 0.87−0.93 (m, 24H), 1.34−1.54 (m, 32H), 1.85−1.89 (m, 16H), 2.36 (s, br, 12H),

dx.doi.org/10.1021/ic4025052 | *Inorg. Chem.* 2014, 53, 737−745

4.08 (t, J = 6.8 Hz, 4H), 5.88 (s, 4H), 6.09 (s, 4H), 6.93−6.95 (m, 16H), 7.04 (d, J = 8.8 Hz, 4H), 7.32−7.40 (m, 16H), 7.71 (d, J = 8.8 Hz, 4H). ^{13}C NMR (100 MHz, $CDCl_3$) δ: 14.0, 14.1, 22.7, 24.3, 24.3, 24.4, 26.1, 26.9, 29.3, 29.4, 31.9, 52.3, 52.5, 68.3, 84.4, 95.4, 111.7, 114.8, 116.0, 120.3, 123.3, 123.8, 123.9, 125.0, 133.1, 142.4, 143.1, 145.6, 145.9, 159.3. ^{31}P NMR (162 MHz, $CDCl_3$) δ: 4.19 ($^1J_{P-Pt}$ = 2345 Hz). IR (KBr): 2091 (C≡C) cm^{-1}. HRMS calcd for $C_{128}H_{136}O_2P_2Pt$: 1961.9663. Found: 1961.9677.

Complex ***C3***. Pale yellow solids: yield 60%; mp 280 °C (with decomposition). ^{1}H NMR (400 MHz, $CDCl_3$) δ: 0.93−1.04 (m, 24H), 1.37−1.42 (m, 16H), 1.47−1.58 (m, 16H), 1.62−1.71 (m, 12H), 1.98−2.17 (m, 4H), 2.20−2.24 (m,12H), 3.94 (t, J = 6.8 Hz, 4H), 5.67 (s, 4H), 5.85 (s, 4H), 6.90−6.95 (m, 16H), 7.29−7.31 (m, 8H), 7.33−7.40 (m, 12H), 7.61 (d, J = 8.0 Hz, 4H). ^{13}C NMR (100 MHz, $CDCl_3$) δ: 14.1, 14.3, 22.9, 24.1, 24.3, 24.6, 24.6, 24.7, 26.5, 26.6, 29.5, 29.7, 30.7, 32.1, 48.3, 52.5, 76.1, 94.3, 119.7, 123.3, 123.8, 125.0, 130.7, 131.2, 135.2, 144.9, 145.1, 145.5, 149.4. ^{31}P NMR (162 MHz, $CDCl_3$) δ: 3.53 ($^1J_{P-Pt}$ = 2342 Hz). IR (KBr): 2098 (C≡C) cm^{-1}. HRMS calcd for $C_{128}H_{136}O_2P_2Pt$: 1961.9663. Found: 1961.9669.

Complex ***C4***. Pale yellow solids: yield, 65%; mp, 124 °C. ^{1}H NMR (400 MHz, $CDCl_3$) δ: 0.86−0.93 (m, 24H), 1.28−1.31 (m, 16H), 1.39−1.48 (m, 16H), 1.52−1.59 (m, 12H), 1.75−1.79 (m, 4H), 2.09−2.16 (m, 12H), 3.95 (t, J = 6.4 Hz, 4H), 6.83 (d, J = 7.6 Hz, 4H), 7.19 (d, J = 7.2 Hz, 4H), 7.32 (d, J = 7.6 Hz, 4H), 7.41 (d, J = 8.8 Hz, 4H). ^{13}C NMR (100 MHz, $CDCl_3$) δ: 14.0, 14.3, 22.8, 23.9, 24.0, 24.2, 24.46, 24.52, 24.59, 26.1, 26.5, 29.31, 29.34, 29.5, 31.9, 68.1, 88.5, 114.4, 115.3, 130.5, 130.9, 132.7, 158.8. ^{31}P NMR (162 MHz, $CDCl_3$) δ: 3.33 ($^1J_{P-Pt}$ = 2350 Hz). IR (KBr): 2095 (C≡C) cm^{-1}. HRMS calcd for $C_{72}H_{104}O_2P_2Pt$: 1257.7159. Found: 1257.7158.

■ ASSOCIATED CONTENT

Ⓢ Supporting Information

Detailed synthetic schemes and procedures; characterization data of new compounds; ^{1}H, ^{13}C, and ^{31}P NMR spectra of **C1**−**C4**; CV and DPV profiles of the ligands; DFT-optimized structures and data of **C2** and **C4**; and the Cartesian coordinates of optimized structures for **C1**−**C4**. This material is available free of charge via the Internet at http://pubs.acs.org.

■ AUTHOR INFORMATION

Corresponding Author

*E-mail: jsyang@ntu.edu.tw.

Notes

The authors declare no competing financial interest.

■ ACKNOWLEDGMENTS

We thank the National Science Council of Taiwan, ROC, and National Taiwan University (Excellence Research Project 102R891303) for financial support. We appreciate Mr. Chen-Yi Kao for the support of photography. The computing time granted by the National Center of High-Performance Computing and the Computing Center of NTU is also acknowledged.

■ REFERENCES

(1) Feng, Y.; Cheng, J.; Zhou, L.; Zhou, X.; Xiang, H. *Analyst* **2012**, *137*, 4885−4901.
(2) Zhao, J.; Wu, W.; Sun, J.; Guo, S. *Chem. Soc. Rev.* **2013**, *42*, 5323−5351.
(3) Kozhevnikov, D. N.; Kozhevnikov, V. N.; Shafikov, M. Z.; Prokhorov, A. M.; Bruce, D. W.; Williams, J. A. G. *Inorg. Chem.* **2011**, *50*, 3804−3815.
(4) Liu, Y.; Guo, H.; Zhao, J. *Chem. Commun.* **2011**, *47*, 11471−11473.
(5) To, W.-P.; Tong, G. S.-M.; Lu, W.; Ma, C.; Liu, J.; Chow, A. L.-F.; Che, C.-M. *Angew. Chem., Int. Ed.* **2012**, *51*, 2654−2657.
(6) Zhang, G.; Palmer, G. M.; Dewhirst, M. W.; Fraser, C. L. *Nat. Mater.* **2009**, *8*, 747−751.
(7) Kostov, Y.; Rao, G. *Sens. Actuators, B* **2003**, *90*, 139−142.
(8) McLaurin, E. J.; Greytak, A. B.; Bawendi, M. G.; Nocera, D. G. *J. Am. Chem. Soc.* **2009**, *131*, 12994−13001.
(9) Yoshihara, T.; Yamaguchi, Y.; Hosaka, M.; Takeuchi, T.; Tobita, S. *Angew. Chem., Int. Ed.* **2012**, *51*, 4148−4151.
(10) Xiang, H.; Zhou, L.; Feng, Y.; Cheng, J.; Wu, D.; Zhou, X. *Inorg. Chem.* **2012**, *51*, 5208−5212.
(11) Liu, X.; Sun, W.; Zou, L.; Xie, Z.; Li, X.; Lu, C.; Wang, L.; Cheng, Y. *Dalton Trans.* **2012**, *41*, 1312−1319.
(12) Wong, K. M.-C.; Yam, V. W.-W. *Coord. Chem. Rev.* **2007**, *251*, 2477−2488.
(13) Wong, K. M.-C.; Yam, V. W.-W. *Acc. Chem. Res.* **2011**, *44*, 424−434.
(14) Kalinowski, J.; Fattori, V.; Cocchi, M.; Williams, J. A. G. *Coord. Chem. Rev.* **2011**, *255*, 2401−2425.
(15) Chou, P.-T.; Chi, Y.; Chung, M.-W.; Lin, C.-C. *Coord. Chem. Rev.* **2011**, *255*, 2653−2665.
(16) Bacon, J. R.; Demas, J. N. *Anal. Chem.* **1987**, *59*, 2780−2785.
(17) Kavandi, J.; Callis, J.; Gouterman, M.; Khalil, G.; Wright, D.; Green, E.; Burns, D.; McLachlan, B. *Rev. Sci. Instrum.* **1990**, *61*, 3340−3347.
(18) Carraway, E. R.; Demas, J. N.; DeGraff, B. A.; Bacon, J. R. *Anal. Chem.* **1991**, *63*, 337−342.
(19) Mills, A. *Platinum Met. Rev.* **1997**, *41*, 115−127.
(20) Gouterman, M. *J. Chem. Educ.* **1997**, *74*, 697−702.
(21) Demas, J. N.; DeGraff, B. A. *Coord. Chem. Rev.* **2001**, *211*, 317−351.
(22) Wolfbeis, O. S. *J. Mater. Chem.* **2005**, *15*, 2657−2669.
(23) DeGraff, B. A.; Demas, J. N. In *Reviews in Fluorescence 2005*; Geddes, C., Lakowicz, J., Eds.; Springer: New York, 2005; Vol. *2005*, pp 125−151.
(24) Stich, M. I. J.; Fischer, L. H.; Wolfbeis, O. S. *Chem. Soc. Rev.* **2010**, *39*, 3102−3114.
(25) Rogers, J. E.; Cooper, T. M.; Fleitz, P. A.; Glass, D. J.; McLean, D. G. *J. Phys. Chem. A* **2002**, *106*, 10108−10115.
(26) Liu, Y.; Jiang, S.; Glusac, K.; Powell, D. H.; Anderson, D. F.; Schanze, K. S. *J. Am. Chem. Soc.* **2002**, *124*, 12412−12413.
(27) Yang, J.-S.; Yan, J.-L. *Chem. Commun.* **2008**, 1501−1512.
(28) Yang, J.-S.; Yan, J.-L.; Lin, C.-K.; Chen, C.-Y.; Xie, Z.-Y.; Chen, C.-H. *Angew. Chem., Int. Ed.* **2009**, *48*, 9936−9939.
(29) Yang, J.-S.; Swager, T. M. *J. Am. Chem. Soc.* **1998**, *120*, 11864−11873.
(30) Thomas, S. W.; Joly, G. D.; Swager, T. M. *Chem. Rev.* **2007**, *107*, 1339−1386.
(31) Zhao, X.; Cardolaccia, T.; Farley, R. T.; Abboud, K. A.; Schanze, K. S. *Inorg. Chem.* **2005**, *44*, 2619−2627.
(32) Sonogashira, K.; Yatake, T.; Tohda, Y.; Takahashi, S.; Hagihara, N. *J. Chem. Soc., Chem. Commun.* **1977**, 291−292.
(33) Yang, J.-S.; Yan, J.-L.; Hwang, C.-Y.; Chiou, S.-Y.; Liau, K.-L.; Tsai, H.-H. G.; Lee, G.-H.; Peng, S.-M. *J. Am. Chem. Soc.* **2006**, *128*, 14109−14119.
(34) Glusac, K.; Köse, M. E.; Jiang, H.; Schanze, K. S. *J. Phys. Chem. B* **2007**, *111*, 929−940.
(35) Glimsdal, E.; Dragland, I.; Carlsson, M.; Eliasson, B.; Melø, T. B.; Lindgren, M. *J. Phys. Chem. A* **2009**, *113*, 3311−3320.
(36) Rausch, A. F.; Homeier, H. H. H.; Yersin, H. *Top. Organomet. Chem.* **2010**, *29*, 193−235.
(37) Yersin, H.; Rausch, A. F.; Czerwieniec, R.; Hofbeck, T.; Fischer, T. *Coord. Chem. Rev.* **2011**, *255*, 2622−2652.
(38) Silverman, E. E.; Cardolaccia, T.; Zhao, X.; Kim, K.-Y.; Haskins-Glusac, K.; Schanze, K. S. *Coord. Chem. Rev.* **2005**, *249*, 1491−1500.
(39) Cooper, T. M.; Krein, D. M.; Burke, A. R.; McLean, D. G.; Rogers, J. E.; Slagle, J. E.; Fleitz, P. A. *J. Phys. Chem. A* **2006**, *110*, 4369−4375.
(40) Becke, A. D. *J. Chem. Phys.* **1993**, *98*, 5648−5652.

(41) Lee, C.; Yang, W.; Parr, R. G. *Phys. Rev. B* **1988**, *37*, 785−789.
(42) Becke, A. D. *Phys. Rev. A* **1988**, *38*, 3098−3100.
(43) Andrae, D.; Häussermann, U.; Dolg, M.; Stoll, H.; Preuss, H. *Theor. Chim. Acta.* **1990**, 123−141.
(44) Levitus, M.; Schmieder, K.; Ricks, H.; Shimizu, K. D.; Bunz, U. H. F.; Garcia-Garibay, M. A. *J. Am. Chem. Soc.* **2001**, *123*, 4259−4265.
(45) Evans, D. H.; Gilicinski, A. G. *J. Phys. Chem.* **1992**, *96*, 2528−2533.
(46) Kraiya, C.; Singh, P.; Evans, D. H. *J. Electroanal. Chem.* **2004**, *563*, 203−212.
(47) Tao, C.-H.; Zhu, N.; Yam, V. W.-W. *Chem.—Eur. J.* **2005**, *11*, 1647−1657.
(48) Lakowicz, J. R. In *Principles of Fluorescence Spectroscopy*, 3rd ed.; Springer: New York, 2006; pp 277−318.
(49) Lakowicz, J. R.; Weber, G. *Biochemistry* **1973**, *12*, 4161−4170.
(50) Iiba, E.; Hirai, K.; Tomioka, H.; Yoshioka, Y. *J. Am. Chem. Soc.* **2002**, *124*, 14308−14309.
(51) Mills, A. *Sens. Actuators, B* **1998**, *51*, 60−68.
(52) Köse, M. E.; Carroll, B. F.; Schanze, K. S. *Langmuir* **2005**, *21*, 9121−9129.
(53) McDonagh, C.; Burke, C. S.; MacCraith, B. D. *Chem. Rev.* **2008**, *108*, 400−422.
(54) Wang, X.-D.; Wolfbeis, O. S. *Anal. Chem.* **2013**, *85*, 487−508.
(55) Dawson, W. R.; Windsor, M. W. *J. Phys. Chem.* **1968**, *72*, 3251−3260.
(56) Frisch, M. J.; Trucks, G. W.; Schlegel, H. B.; Scuseria, G. E.; Robb, M. A.; Cheeseman, J. R.; Scalmani, G.; Barone, V.; Mennucci, B.; Petersson, G. A.; Nakatsuji, H.; Caricato, M.; Li, X.; Hratchian, H. P.; Izmaylov, A. F.; Bloino, J.; Zheng, G.; Sonnenberg, J. L.; Hada, M.; Ehara, M.; Toyota, K.; Fukuda, R.; Hasegawa, J.; Ishida, M.; Nakajima, T.; Honda, Y.; Kitao, O.; Nakai, H.; Vreven, T.; Montgomery, J. A.; Peralta, J. E.; Ogliaro, F.; Bearpark, M.; Heyd, J. J.; Brothers, E.; Kudin, K. N.; Staroverov, V. N.; Kobayashi, R.; Normand, J.; Raghavachari, K.; Rendell, A.; Burant, J. C.; Iyengar, S. S.; Tomasi, J.; Cossi, M.; Rega, N.; Millam, J. M.; Klene, M.; Knox, J. E.; Cross, J. B.; Bakken, V.; Adamo, C.; Jaramillo, J.; Gomperts, R.; Stratmann, R. E.; Yazyev, O.; Austin, A. J.; Cammi, R.; Pomelli, C.; Ochterski, J. W.; Martin, R. L.; Morokuma, K.; Zakrzewski, V. G.; Voth, G. A.; Salvador, P.; Dannenberg, J. J.; Dapprich, S.; Daniels, A. D.; Farkas, O.; Foresman, J. B.; Ortiz, J. V.; Cioslowski, J.; Fox, D. J. *Gaussian, Revision A.02*; Gaussian, Inc.: Wallingford, CT, 2009.